VELOCITY, INTERFACE COMPLEXITY AND DROPLETS PRODUCTION IN THE NEAR NOZZLE REGION OF A DIESEL SPRAY: COMPARISON BETWEEN EXPERIMENTAL ANALYSIS AND DIRECT NUMERICAL SIMULATION

K. Lounnaci, S. Idlahcen, T. Menard, Claude Rozé, J. Blaisot

VELOCITY, INTERFACE COMPLEXITY AND DROPLETS PRODUCTION IN THE NEAR NOZZLE REGION OF A DIESEL SPRAY: COMPARISON BETWEEN EXPERIMENTAL ANALYSIS AND DIRECT NUMERICAL SIMULATION

K. LOUNNACI[c], S. IDLAHCEN, T. MENARD, C. ROZE, J.B. BLAISOT

CORIA UMR 6614 - Normandie Université - CNRS - Université et INSA de Rouen, Campus Universitaire du Madrillet
76800 Saint Etienne du Rouvray, France.
[c]Corresponding author: Email: kamel.lounnaci@coria.fr

KEYWORDS:
Main subjects: flow visualization, image processing.
Fluid: Diesel spray, high speed flows.
Visualization method(s): ultrafast shadow imaging, double-pulsed femtosecond laser system.
Other keywords: atomization, velocity, experimental analysis, direct numerical simulation.

ABSTRACT: *A transillumination imaging arrangement using a double-pulsed femtosecond laser system coupled to a double frame camera was used to record high-resolution time-correlated image-pairs in the near-nozzle region of a high pressure Diesel jet. On the other hand, direct numerical simulations (DNS) using coupled volume of fluid/level set (VOF/LS) method for interface tracking have been carried out for this kind of injection. For the sake of precision of these numerical simulations, the flow inside the injector was also computed by using a commercial CFD code (Fluent 6.3). A quantitative comparison between numerical simulations and experimental images has been performed by applying the same tools. From the numerical point of view, some jet characteristics are well reproduced and this study allowed detecting the features that need improvement.*

1 Introduction

The reduction in emitted pollutants from the liquid fueled internal combustion engines requires a complete understanding of the combustion process within these engines. The fuel injection is a key factor, as it determines the drop size distribution, which influences the liquid evaporation rate and the fuel-air mixture efficiency in the chamber. Even if the general trend in Diesel applications is to increase the injection pressure (up to 200 MPa) and to decrease the orifice diameter (down to 100 µm), as these two parameters seem to improve engine efficiency, the spray break up is not yet fully understood. The main reason is that the form and distribution of liquid structures in the spray is the result of a lot of interdependent and complex processes (hydrodynamic instability, cavitation, turbulence, etc.) [1], which complicate analysis of atomization phenomena and frustrate direct control of the spray formation. Significant progresses have been made recently for the numerical simulation of injection. Direct numerical simulation (DNS) can now produce realistic results. Nevertheless, it is necessary to move beyond the simple visual comparison to more quantitative validation.
The objective of this paper is to quantitatively compare experimental and numerical observations by applying the same tools on the numerical simulations and on experimental images. The quantities used for the comparison are: liquid flow velocity, atomization progress and deformation of the liquid/gas

interface. From the experimental point of view, these quantities were obtained from to a large set of images, to extract statistically valid trends. The sprays used in this work were produced by a single-hole, plain orifice injector assembly dispersing fuel oil into ambient atmospheric conditions. The velocity data and shadow images of the Diesel spray used in the analysis were obtained using high-resolution ultrafast shadow imaging (USI) [2, 3], which provides highly resolved visualization of the spray edges and droplets, resolved within a narrow depth-of-field.

The experimental results were confronted with DNS computations for a similar liquid jet. A coupled volume of fluid/level set (VOF/LS) method was used for interface tracking. The incompressible Navier-Stokes equations were solved following a projection method and coupled to a transport equation for the level set function on a Cartesian meshing [4, 5]. In order to provide the characteristics of the flow at the nozzle orifice for DNS computations, the internal flow was computed using a commercial CFD code (Fluent 6.3), based on the geometry deduced from X-ray imaging of the nozzle used in the experiments. The results of the numerical simulations were transformed into images by plane projection.

Finally, comparisons between experimental results and numerical simulations lead to contrasting conclusions. Some jet features were well reproduced by the computations. Improvement in DNS is nevertheless expected to fully mimic the jet behavior.

2 Experimental setup

From an experimental point of view, the visualization of Diesel injection in the near field of the nozzle is a challenge. Indeed, because of the high injection pressure, the liquid velocity reaches several hundred of $m.s^{-1}$. The region of interest covers a few millimetres from the nozzle exit, which necessitates a high optical magnification. Moreover, the high optical density of the liquid jet complicates the visualization of the spray. A transillumination imaging arrangement (see Fig. 1 (a)) was developed to extract high-resolution visual information from limited areas of the spray in the near-nozzle region (see Fig. 1 (b)) [2, 3].

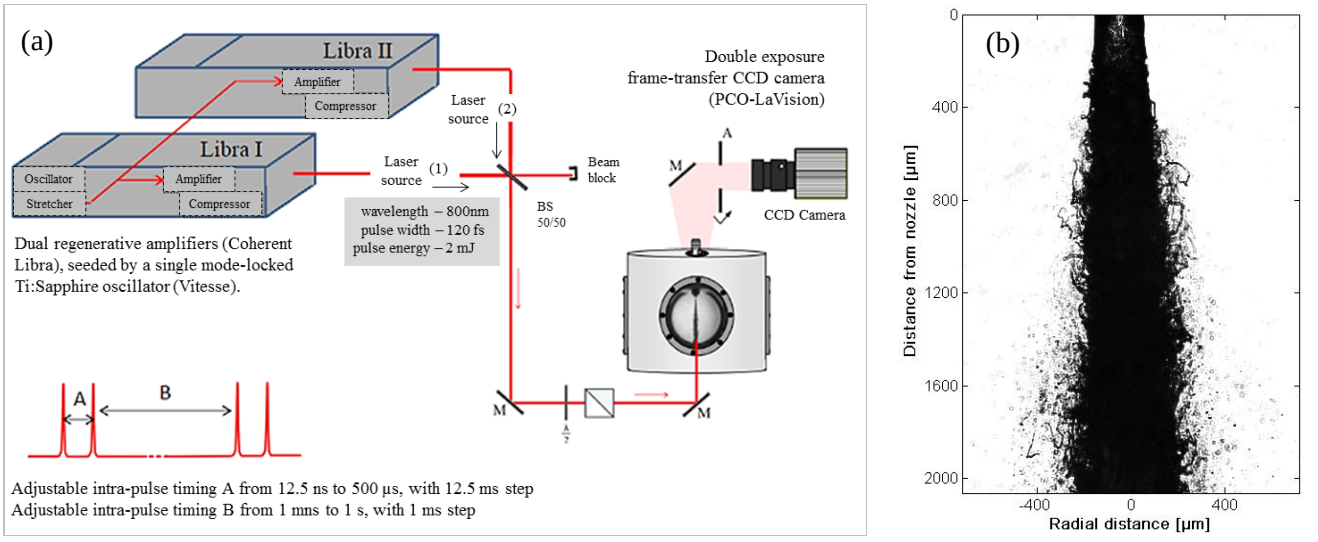

Fig. 1 (a) Experimental setup (high-resolution ultrafast shadow imaging), (b) example of a Diesel jet visualisation.

The light source used to image the spray was a double-pulsed femtosecond system consisting of a pair of matched regenerative Ti-Sapphire amplifiers (Coherent Libra, 1 kHz) seeded by a common oscillator (Coherent Vitesse, 80 MHz). The femtosecond pulse of the oscillator was stretched and separated into two beams, which were subsequently strengthened in the cavity of each amplifier. After compression, the two beams were combined into a single beam, containing a matched pair of pulses. By selecting the specific pair of oscillator pulses to amplify, the delay between the two output pulses was adjustable from 12.5 ns to 500 µs, with an accuracy of a few picoseconds, due to minute path differences between the selected seed pulses.
Here, the adjustment step size of 12.5 ns corresponds to the period of the oscillator. The duration of each pulse was 120 fs, which was sufficient to freeze the spray motion during the measurement, such that time-resolved images were acquired. The laser system was carefully aligned to obtain similar profiles in each pulse-pair, in terms of duration, amplitude, optical alignment, polarization, and spatial profile. The beam diameter was ~10 mm, with a low divergence, a center wavelength of 800 nm and the energy per pulse on the order of 3.7 mJ.
The two-pulse beam was directed across a chamber housing the injector to illuminate the spray. The chamber was ventilated and maintained at ambient conditions; optical access was provided by thin fused-silica windows to prevent contamination of the optical components by fuel.
The transmitted light was collected to form images on the face of a double-image CCD (PCO, 2560 × 2160 pixels), and the imaging system was equipped with a long distance microscope allowing ~7× magnification of the spray images. The scale of the resulting spatial intensity data was 1040 pixels/mm, and the resolution of the complete imaging system was on the order of 4.2 µm.
The fluid used in the measurements was a calibration oil (Shell NormaFluid, ISO 4113) with properties similar to Diesel fuel and precisely controlled viscosity, density and surface tension specifications (see Table 1) [6].

Density	Viscosity	Surface Tension
821 $kg.m^{-3}$	0.0032 $kg.m^{-1}.s^{-1}$	0.02547 $N.m^{-1}$

Table 1 Thermophysical properties of ISO 4113 oil.

The injector used in the measurements were installed in a 3-axis translation stage and supplied by a pump through a common-rail accumulator. This injector produces a uniform flow. The test nozzle and injection parameters are summarized in Table 2.

Discharge coefficient	Length to diameter ratio	Needle lift	Back pressure	Injection pressure
0.86	5.16	100 µm	0.1 MPa	30 MPa

Table 2 Test nozzle and injection parameters.

3 Numerical methods

3.1 Internal flow simulation

The DNS of the primary breakup requires knowing the characteristics of the flow at the nozzle orifice. However, these data cannot be obtained experimentally, especially for the study of high pressure Diesel

injection. Thus, the internal flow was computed using a commercial CFD code (Fluent 6.3). This numerical study was carried out using the thermophysical properties of Normafluid listed in Table 1 and the spray properties and injection parameters as in Table 2. It should be noted that the fluctuating pressure conditions and the cavitation inside the injector were not considered in the computation. However, the chosen injection parameters limit these effects.

The internal geometry of the nozzle used in the present study was measured from X-ray imaging. Three X-ray images have been taken of the nozzle every 45° (see Fig. 2) in order to conclude on the axisymmetric nature of the injector and to create the most realistic three-dimensional mesh. On each X-ray image, a Sobel gradient filter was applied to detect the edges of the nozzle. The internal geometry of the injector was made by using Gambit 2.4 (see Fig. 3).

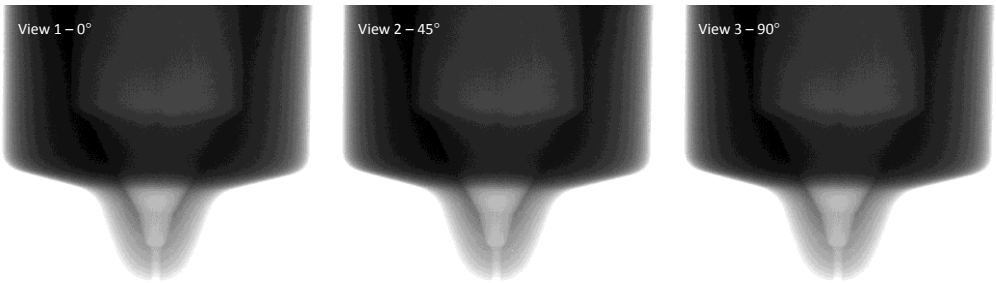

Fig. 2 X-ray transmission shadowgrams showing internal geometry at different orientations.

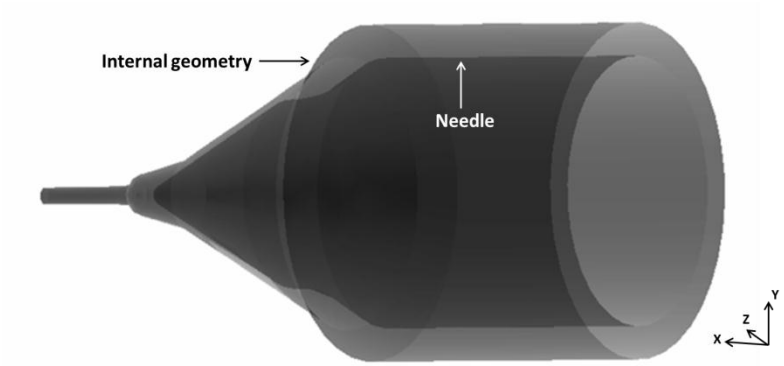

Fig. 3 Internal geometry of the nozzle at needle lift to 100 µm used in the internal flow computation.

Meshing the domain is an important step in this kind of study, indeed the simulation results directly depend on the quality of the numerical grid. Thereby a preliminary study on the mesh influence was carried out. Four different grids were used on the same geometry; 69917 cells, 280297 cells, 382155 cells and 501823 cells. Due to the complexity of the nozzle internal geometry, all the cells are tetrahedral. The standard (STD) k-ε model usually gives quite reasonable results in the cases of high Reynolds number flow. Nevertheless, in some cases, e.g. high velocity flow, this model gives a too large turbulent diffusivity and leads to an unrealistic flow behaviour. The RNG k-ε model was developed using Re-Normalisation Group (RNG) methods [7]. The RNG approach consists in the modification of the production coefficient, which allows to account for the different scales of motion in the turbulent diffusion unlike the STD k-ε model. The internal injector flow was computed with this more efficient method.

The influence of the mesh was carefully checked. Fig. 4 shows the evolution of the mass flow at the nozzle orifice for four meshes. It was found that from approximately 300000 cells the simulation results reach an asymptotic behavior. The results presented in this section are derived from the mesh to 382155 cells. Fig. 5 shows the corresponding mesh.

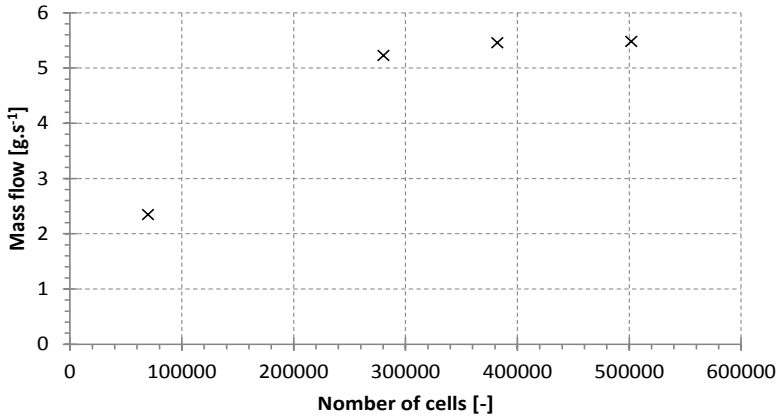

Fig. 4 Mass flow evolution for four different meshes.

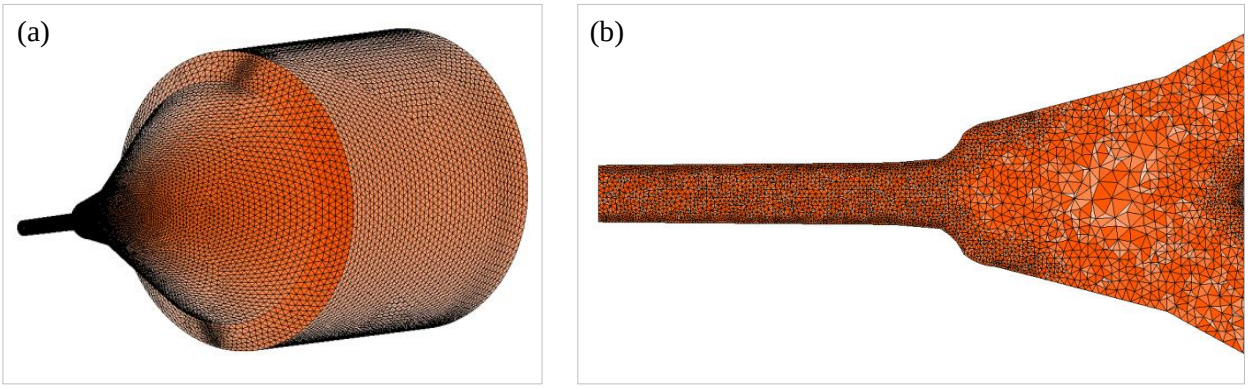

Fig. 5 (a) Overview of the mesh to 382155 cells, (b) section view of cells near the nozzle exit.

This preliminary numerical study allowed obtaining the characteristics of the flow at the nozzle orifice. These data were used as input conditions for the DNS of the external flow, in order to compare the primary breakup with the experimental data. Fig. 6 shows the velocity magnitude field at the nozzle orifice. The velocity at injector outlet is about 250 m/s, which is realistic compared to the experimental velocity evaluations, which are presented in a next section.

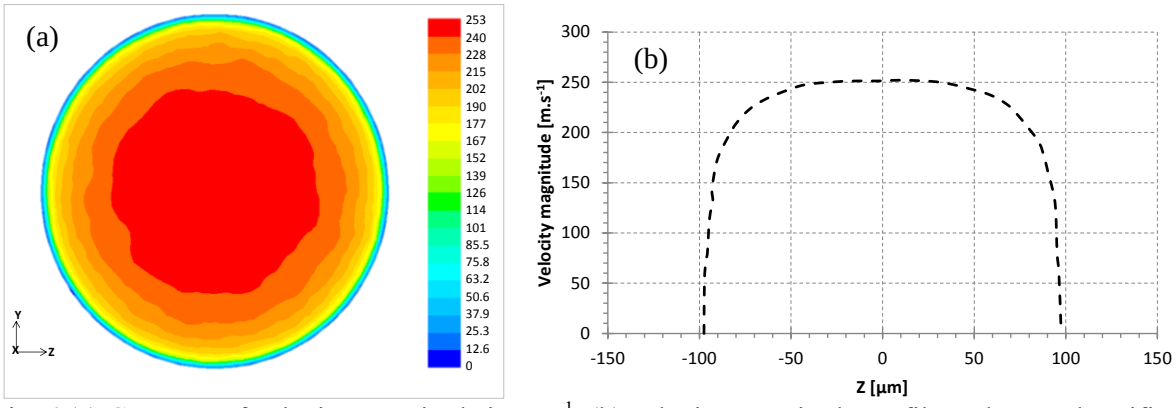

Fig. 6 (a) Contours of velocity magnitude in $m.s^{-1}$, (b) velocity magnitude profile at the nozzle orifice.

3.2 Direct numerical simulation of external flow

Numerical simulations were performed with two phase flow computation code (ARCHER [8]) using Coupled Level Set and Volume Of Fluid (CLSVOF) method [9] to track the interface. Inlet conditions were imposed using previous computation and Klein method to introduce uniformly both length scale and intensity of turbulence [10]. The first is taken to 8% of jet diameter and the second to 5 % of the inlet velocity. The grid dimension was 256 × 256 × 1024 and the mesh size was set to 3 µm.
Fig. 7 (a) shows the image of a 2D projection of the computed jet. Fig. 7 (b) shows the corresponding measured image. The simulated flow maintains the general appearance of the experimental jet, although a number of smaller scale fluid structures, such as the curved ligaments visible at the edges of the measured jet image, were not reproduced in the simulated image.

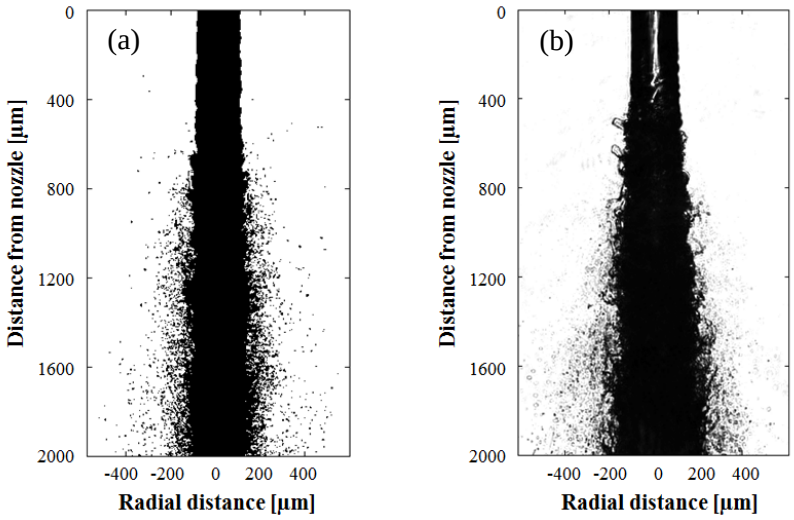

Fig. 7 (a) Simulated jet and (b) experimental image.

Such methods have been shown to be capable of capturing interface instabilities. So that break-up mechanisms can be strongly controlled by the mesh size. Generally it is not possible to capture two interfaces in one cell, and when this phenomenon occurs, break-up of interface is observed. A case of spray numerical simulation shows the influence of mesh size on the drop size distribution [11].

4 Comparison between experiment and simulation results

4.1 Velocity from correlated images-pairs

4.1.1 Description of the method

The experimental data and DNS results discussed in previous sections were processed using an in-house image analysis code based on the OpenCV image processing library [12]. Since the experimental setup described in section 2 allows recording image pairs, a liquid interface from the first image can be detected on the second image. Such image correlation procedure leads to a liquid interface displacement field. Knowing the delay between the images, a velocity map is deduced. The delay (261 ns) between the pulse-pairs in the femtosecond pulse train was adjusted so that the displacement of liquid structures is large enough to be detected but short enough to be sure that the liquid structures of the first image can be recognized on the second one. Fig. 8 shows an image with displacement vectors and an example of an image region pair.

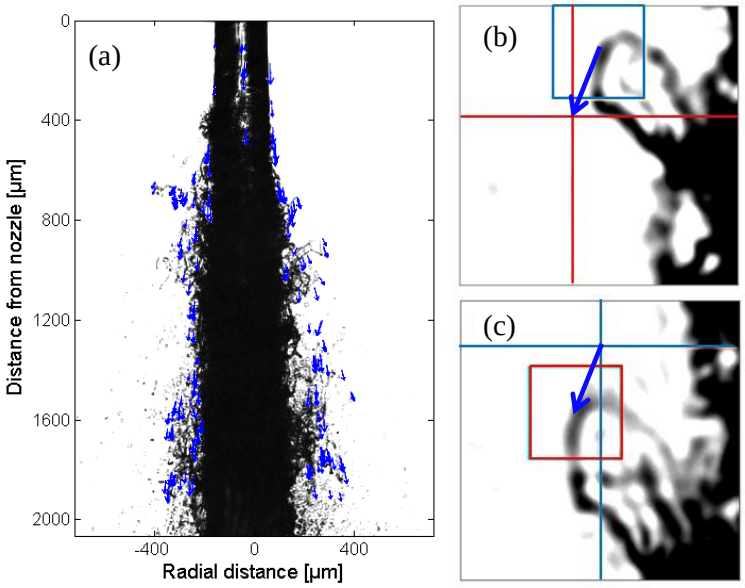

Fig. 8 (a) Image shown with displacement vectors estimated from time-correlated image-pair. Example of an image region pair. The time delay between (b) and (c) is 261 ns.

It is difficult to draw broad conclusions from the velocity map calculated from a single image pair. To extract significant statistical information, a large set of image pairs (500 in this work) were used, individual velocity maps extracted and averaged: the 2560 × 2160 pixels image was divided in to square cells of 20 × 20 pixels and a binning of the velocity vectors performed. For statistical accuracy, all bins containing less than 20 velocity vectors were ignored. Application of this procedure yields an averaged velocity map of the liquid interface. Fig. 9 shows the velocity field of the spray generated by the injector under study.

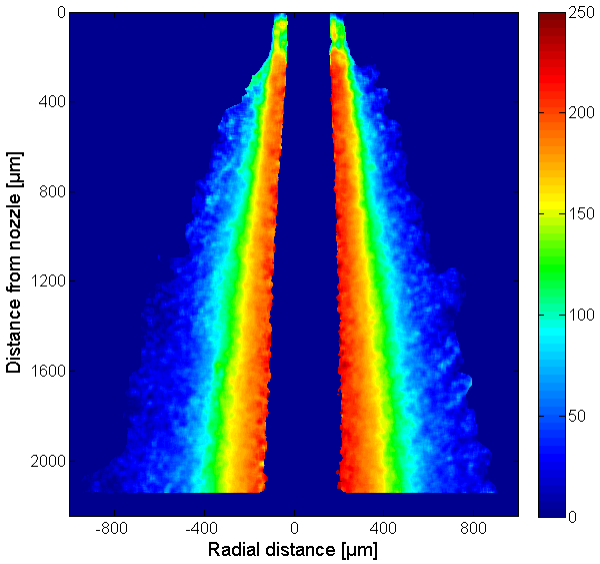

Fig. 9 Velocity map of the spray in $m.s^{-1}$.

In order to have a more detailed analysis of the flow, the individual images of the data set were binarized and segmented into two classes [13], one containing only separated liquid elements (droplets and liquid parcels) and one representing the intact liquid core, as illustrated in Fig. 10. The preceding image processing was then applied separately to the jet core images and to the dispersed elements images, to deduce the respective velocity fields. The binarization method was validated by checking that the velocity results from the original images were the same as the ones computed from the binarized non-segmented images [13]. The resulting maps are given in Fig. 11.

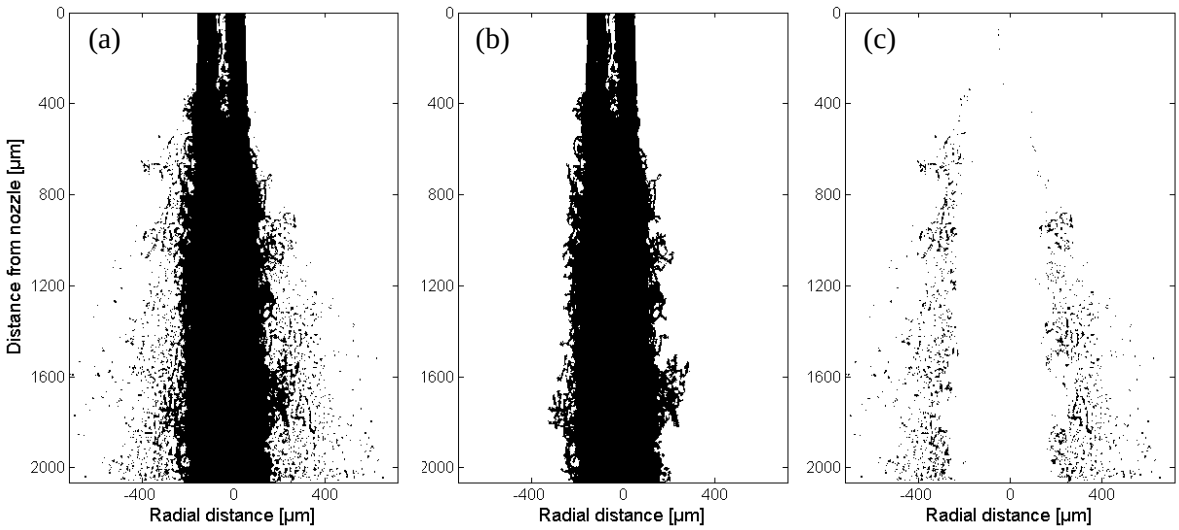

Fig. 10 (a) Image of the flow, (b) jet core and (c) dispersed elements.

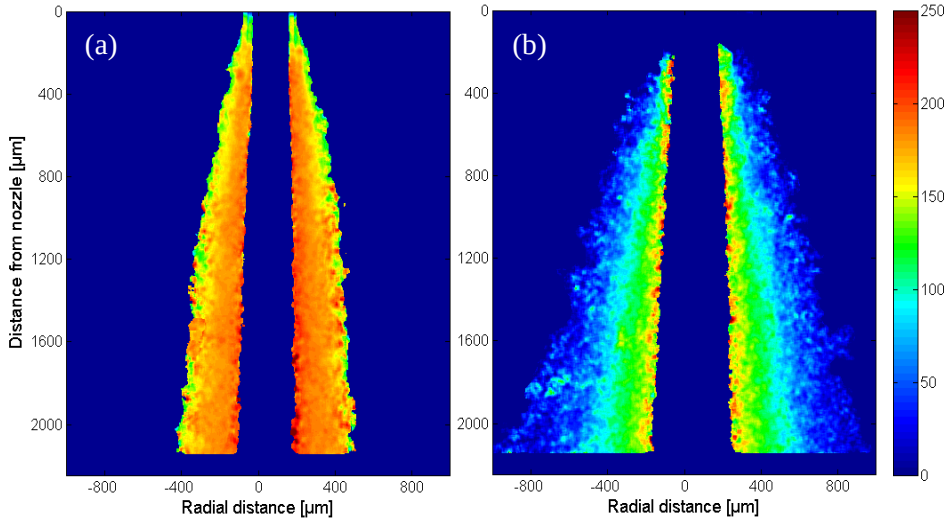

Fig. 11 Mean velocity field in $m.s^{-1}$, (a) of the interface, (b) of dispersed elements.

From the experimental point of view, the observation is limited in 2D, thus the azimuthal velocity component is not taken into account in the results presented previously. Nevertheless, in view of the symmetry of the flow, the latter can be neglected. It must be also noted that the segmentation acts on 2D projections: some droplets or liquid parcels are considered to belong to the liquid core, whereas viewed in 3D, they are separated.

4.1.2 Validity of the method

The interface tracking methods of the atomization simulation offer the possibility of testing the relation between the velocities computed from measurement data and velocities generated under similar conditions by reliable numerical methods. To test the measured velocity results discussed in the previous section, a numerical simulation of a similar spray with an inlet velocity equal to 200 m/s was undertaken. A series of 200 simulated shadowgrams were generated from the numerical data by forming 2D projections of the 3D simulation data with an inter-frame separation time of 200 ns (corresponding to about 270,000 h of CPU time). These time-correlated spatial data were subsequently analyzed using the image correlation procedure applied to the experimental images. In addition, the average radial velocity of the jet surface and droplets was evaluated directly using the 3D simulation data to generate appropriate numerical velocity values for each time step by circular averaging. Fig. 12 plots a comparison of the evaluated interface velocities from the 2D projections of the simulated jet and the velocities given by the 3D simulation data versus the distance to the nozzle. The results are significantly identical. Nevertheless, in the very near field of the nozzle, the interface velocities are badly approximated, indeed in this region the jet is cylindrical and not allows an efficient correlation.

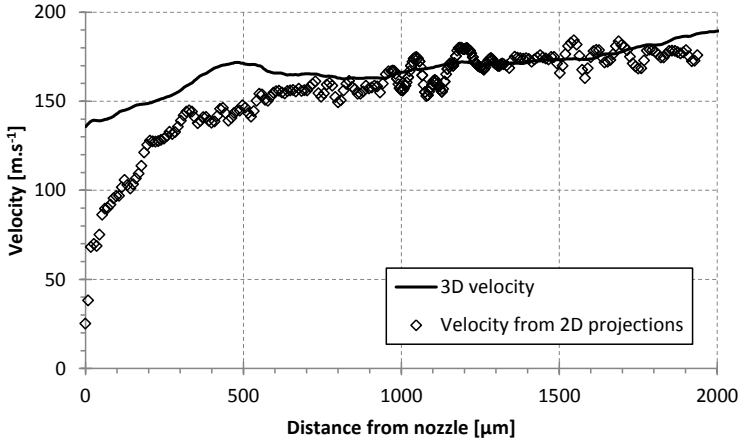

Fig. 12 Comparison of interface velocities evaluated on 2D projections of the simulated jet and the interface velocities given by the 3D simulation data versus the distance to the nozzle.

Fig. 13 plots a comparison of the evaluated droplet velocities from the 2D projections of the simulated jet and the droplet velocities given by the 3D simulation data at different distances from the nozzle. The results show satisfactory agreement between the two procedures, except near the center of the jet, where the droplets are hidden by the liquid core in the 2D projections. These results indicate that the analysis developed for spray images computes reliable vectors that are relevant to the actual velocities describing the motion of the jet interface and droplets in the spray.

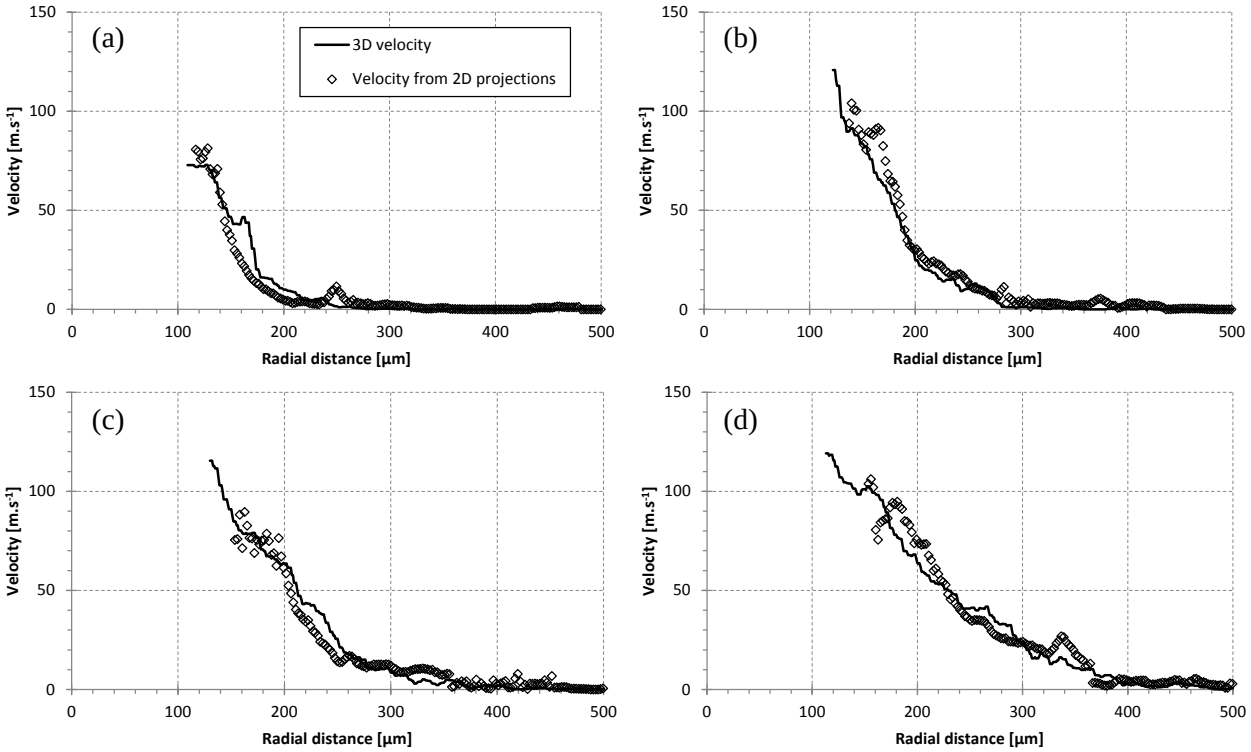

Fig. 13 Comparison of droplet velocities evaluated on 2D projections of the simulated jet and the droplet velocities given by the 3D simulation data. Velocity profiles at 1000 µm from the injector orifice (a), 1500 µm (b), 2000 µm (c) and 2500 µm (d).

4.1.3 Comparison of experimental velocity field with numerical simulation

The experimental velocity field exposed in the first section of this part is compared with the velocity information from the 3D simulation data. To allow a more detailed comparison, the 3D simulation data was separated into two parts; the jet core and the dispersed phase. This segregation applied to the 3D object differs from the experimental procedure, indeed the 2D shadow imaging does not allow to locate the droplets when these are close to the interface. However, as the results shown in Fig. 12 and 13 indicate, the average 3D velocities are comparable to the velocities generated by the image correlation analysis.
The velocity of the jet interface and of the dispersed phase elements was extracted from the numerical simulation data, averaged over the azimuthal angle. Fig. 14 shows these velocity fields.

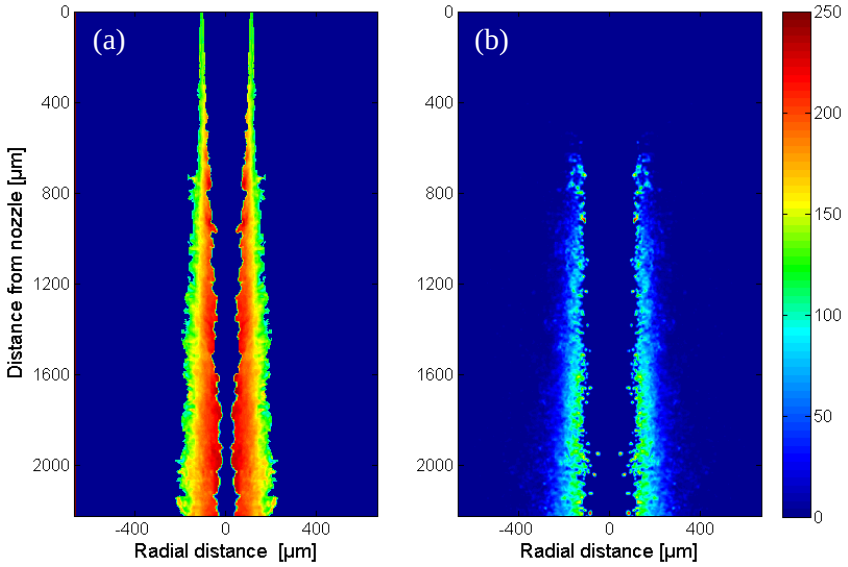

Fig 14 Velocity field in $m.s^{-1}$, (a) of the interface, (b) of dispersed elements obtained from numerical simulations.

The evolution of experimental and numerical interface velocity versus the distance from nozzle are compared in Fig. 15. Here, it is apparent that the liquid core velocity magnitude agrees fairly well with the measurement results, despite the differences between the segregation methods.
The displacement of dispersed elements derived from the atomization is very badly reproduced by the simulation. Indeed, Fig. 16 shows large discrepancies between experimental and simulation droplet velocities. The inlet conditions used to set up the simulations heavily influences the form and trajectories of the dispersed elements. Thus, these discrepancies of velocity are largely the result of an insufficient description of the boundary conditions at the inlet. A research work to improve this point is in progress.

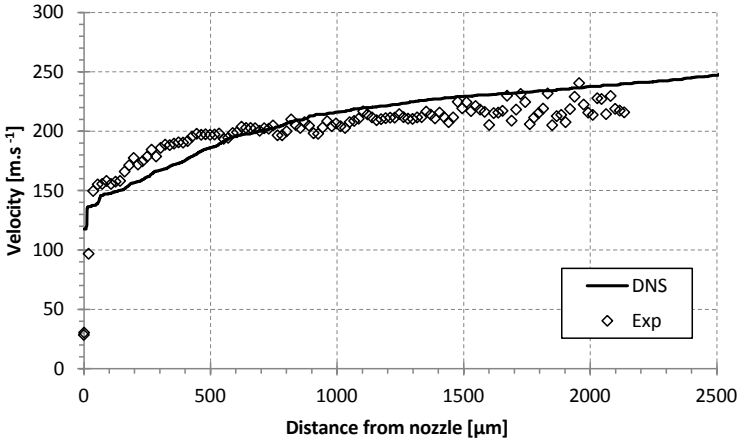

Fig. 15 Comparison of experimental and numerical interface velocity versus the distance from nozzle.

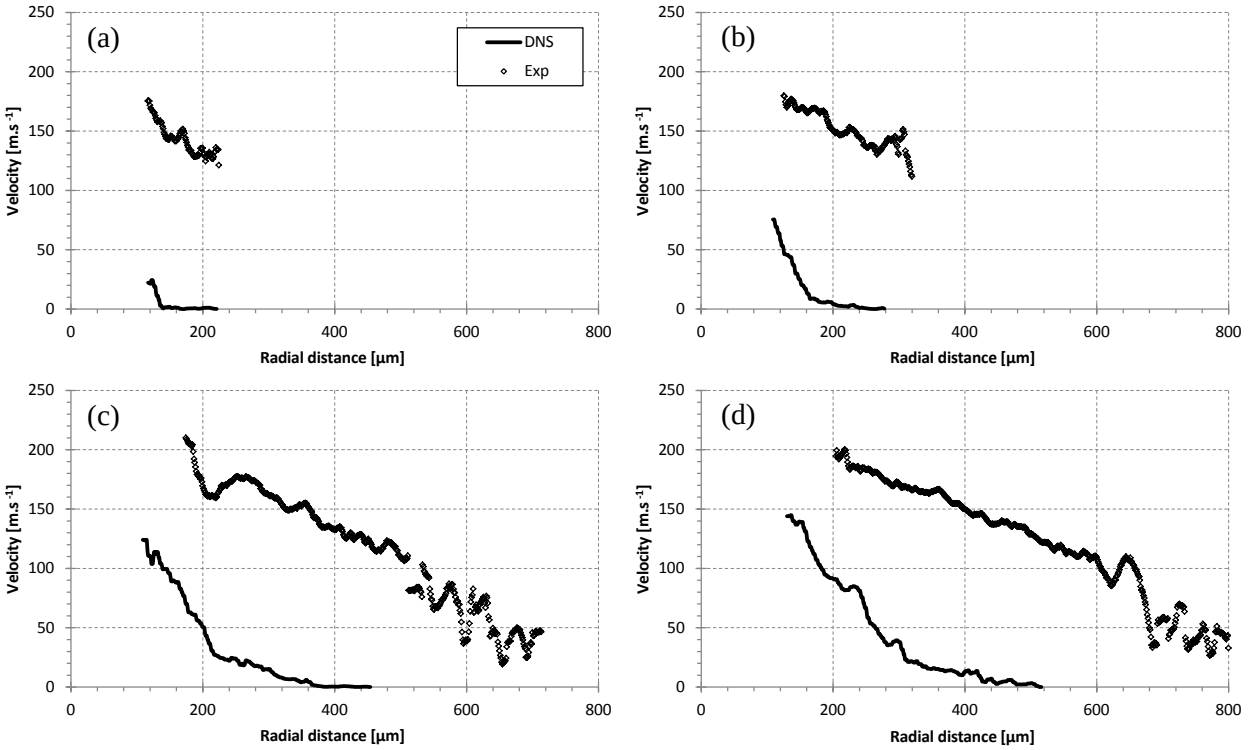

Fig. 16 Comparison of experimental and numerical droplets velocity profiles at different distances from the nozzle: (a) 500 µm, (b) 750 µm, (c) 1500 µm, (d) 200 µm.

4.2 Droplets production

Using sets of separated spatial data, as shown in Fig. 10, three spatial classes can be defined for each pixel: No Liquid (NL), Liquid Core (LC) and Dispersed Phase (DP). In this context, one can make a statistical analysis of the appropriate group of images to calculate the probability, P_{DP}, for each measured region (pixel) to be in state DP. Such analysis leads to the probability field presented in Fig. 17. The experimental result was obtained with 500 images, but the numerical result with 150 images,

which is not sufficient to obtain statistical convergence. Nevertheless, Fig. 18 shows that the simulations correctly reproduce the decreases of the dispersed liquid elements with the radial distance. The amplitudes of the probability differ in the DNS from the experimental data.

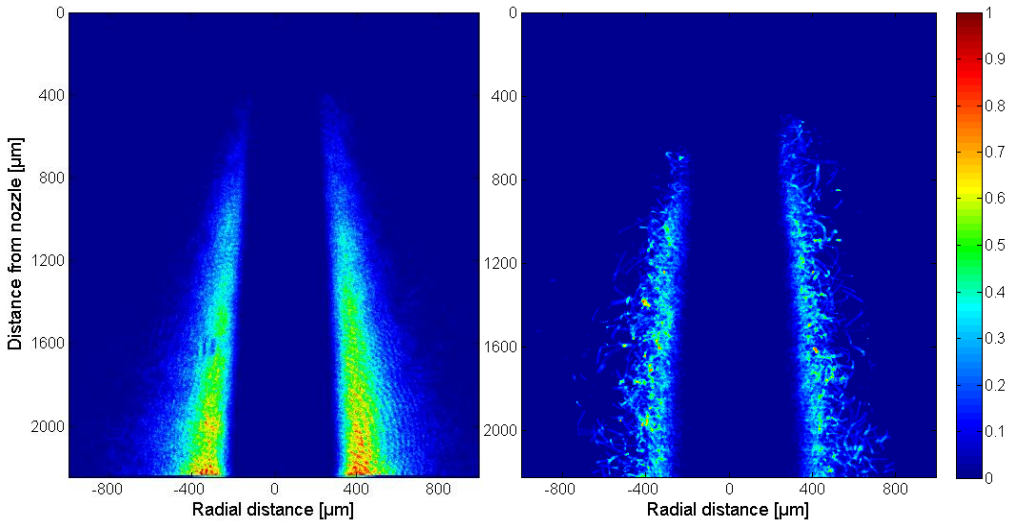

Fig.17 Probability of atomization (based on the projected area) of the experimental jet (a) and of the simulated jet (b).

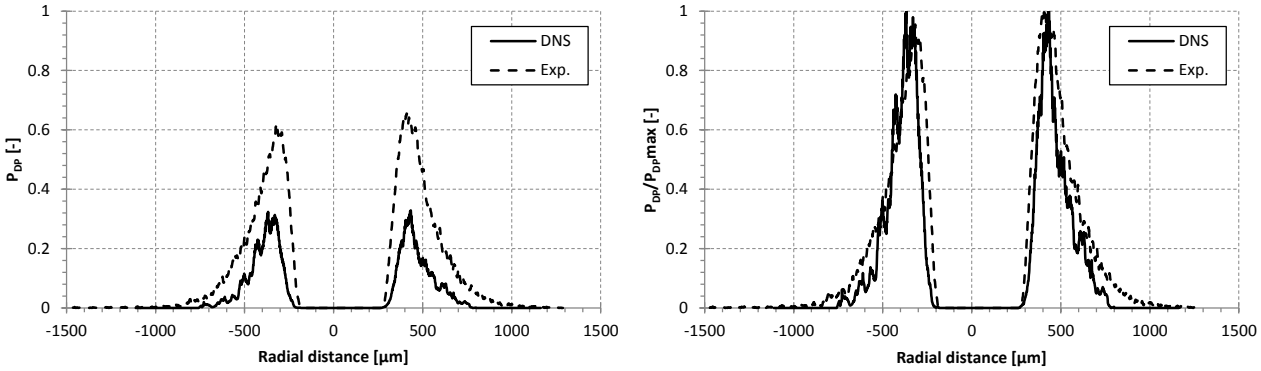

Fig. 18 Profile of probability of atomization at 2000 µm from the injector.

4.3 Jet core interface complexity

The dispersed phase can be characterized by different properties, which have a physical meaning, such as the mean diameter of the liquid elements, the projected area, the probability of presence, etc. The jet core evolves continuously from the nozzle exit to the far field. It can be seen on the images the complexity of the edge increases. In order to make a quantitative evaluation of this evolution, an analysis is necessary, which meets the following conditions: (i) it must be local to follow an evolution along the spray; (ii) it must be an autonomous processing, free of human intervention, to act on a large set of images; (iii) it must be a multi-scale description, because the jet core edges are subject to small deviations but also large curvatures, depending on the observation scale. Different tools are proposed in

the literature: Blaisot and Yon use a morphological description of the jet, based on the measurement of simple shapes (ligaments lengths, etc.) [14]. Shavit and Chigier have characterized Diesel sprays by a fractal dimension [15]. Dumouchel et al develop a sophisticated multi-scale analysis [16]. Nevertheless, none of these methods satisfies all the preceding conditions.
Here, we propose to adapt the description of curves proposed by Mokhtarian et al in the domain of pattern recognition to the jet core images [17]. The principle consists in extracting the curves describing the left and right edges of the jet core by a contour algorithm and to analyze them in terms of curvature distribution along the curve arc-length. More specifically, if one of the edges is described by $(x(s), y(s))$, where s is the arc-length, the curvature along the curve is computed by:

$$\kappa_0(s) = \frac{x'(s)y''(s) - y'(s)x''(s)}{[x'^2(s) + y'^2(s)]^{1.5}} \quad (1)$$

The curve is then smoothed by convolution with a Gaussian of width σ:

$$x_\sigma(s) = x(s) \otimes G(s,\sigma) \text{ and } y_\sigma(s) = y(s) \otimes G(s,\sigma) \quad (2)$$

which acts as a low pass filter. The curvature distribution at scale σ is computed:

$$\kappa_\sigma(s) = \frac{x'_\sigma(s)y''_\sigma(s) - y'_\sigma(s)x''_\sigma(s)}{[x'^2_\sigma(s) + y'^2_\sigma(s)]^{1.5}} \quad (3)$$

When σ increases, the smoothed curve tends to a straight line. The map $\kappa_\sigma(s)$, for $\sigma = 0$ to σ_m, when σ_m is the smallest scale for which the curve is a straight line, is called the Curvature Scale Space (CSS) and is an indicator of the curve complexity at all scales. Fig. 19 shows the computed CSS of the left side contour of the experimental and of the DNS jet.
Deviations are detected on the experimental jet from scales of 1 µm to ~120 µm. For the jet issued from DNS, curvatures are detected for much larger scales.
Extracting general trends from individual images is difficult and thus a CSS averaging was performed: the images were divided into small horizontal strips (of 20 µm height) and all curvatures localized in a given strip were averaged. A second averaging was also performed over the whole set of images. Fig. 20 and Fig. 21 show the average CSS for the experimental jet and the DNS jet respectively. The behavior of the left and right sides of the jet are similar in both cases. A small dissymmetry is just noticeable on the experimental jet. In contrast, the difference between the experimental and the simulated jets is impressive, showing that the primary atomization is not correctly caught by DNS. The complexity increases continuously in the experimental jet, whereas after an abrupt growth, the complexity remains constant in the simulated jet.

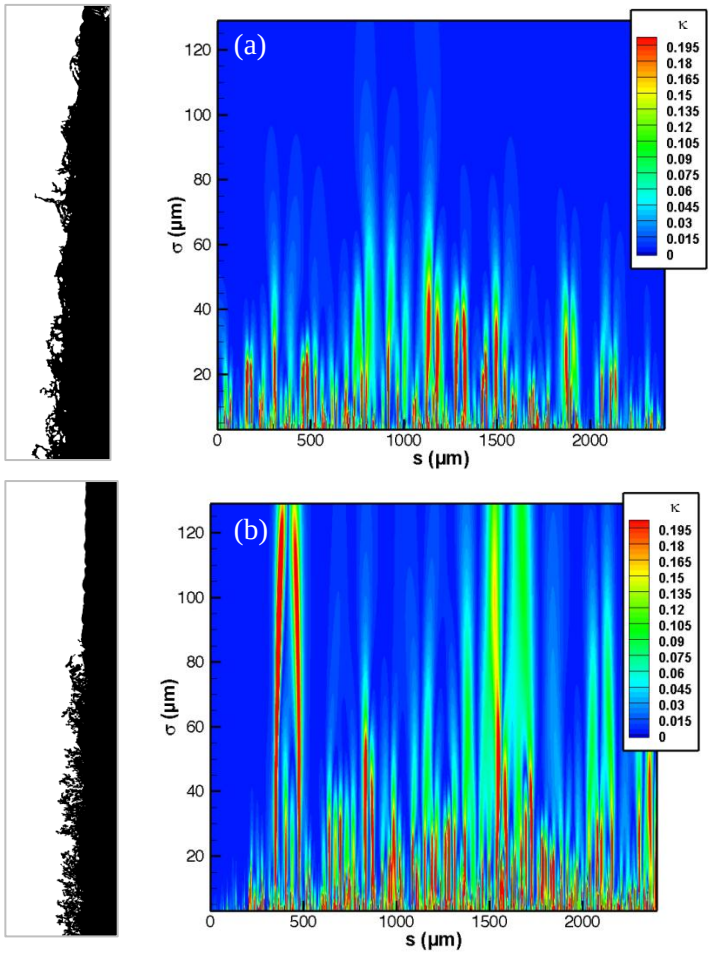

Fig. 19 CSS of the experimental (a) and DNS jet (b). A section of the corresponding edge is shown at left of each diagram. κ in μm^{-1}

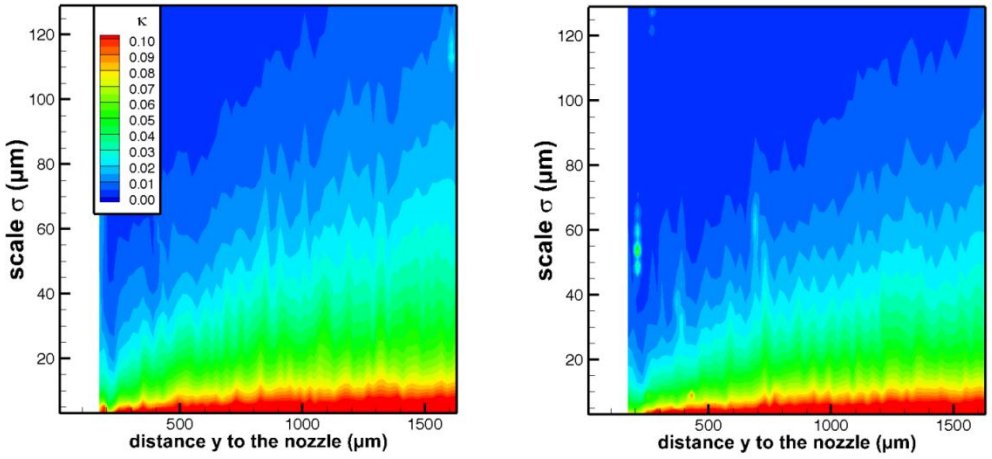

Fig. 20 Averaged left and right side curvature scale distributions for the experiment jet contour (κ in μm^{-1}).

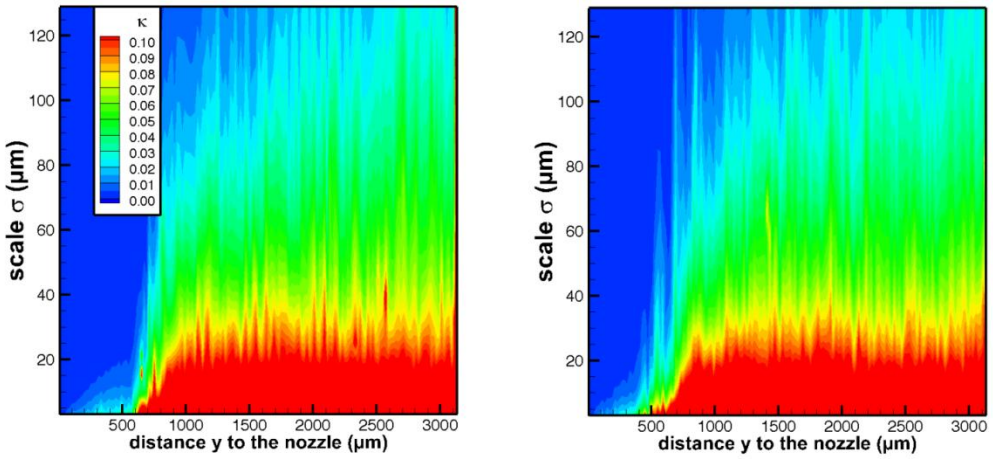

Fig. 21 Averaged left and right side curvature scale distributions for the numerical jet contour (κ in μm^{-1}).

5 Conclusions

There is a strong demand for high-quality spray measurements to validate numerical models of breakup in order to improve the fundamental understanding of the atomization processes. This paper presents a comparative study between experiment analysis and numerical simulations in the case of high pressure Diesel injection.

From the experimental point of view, high resolution time-correlated image-pairs have been obtained by using a transillumination imaging arrangement using a double-pulsed femtosecond laser system coupled to a double frame camera. The sprays used in this work were produced by a single-hole, plain orifice injector assembly dispersing fuel oil into ambient atmospheric conditions. The high resolution of the image data allowed isolating the dispersed liquid elements from the jet core, facilitating a more refined examination of the correlated image structure velocities.

Direct numerical simulations of a high-pressure liquid jet have been carried out, by using a coupled volume of fluid/level set (VOF/LS) method for interface tracking. The internal flow was also computed using a commercial CFD code (Fluent 6.3), based on the geometry deduced from X-ray imaging of the nozzle used in the experiments. This preliminary numerical study provided the characteristics of the flow at the nozzle orifice for DNS computations.

To allow a comparison with the experimental images, the results of the DNS were transformed into images by plane projection.

The experimental velocity data obtained by using correlation images were compared with 3D simulation data. The conclusions of this comparison have been contrasted. Indeed the interface velocity is well reproduced by the computation, unlike the droplet velocities which presents large discrepancies between experimental and simulation results. The simulation must be improved to meet experiments.

The involvements of the 2D limitation imposed by the experimental visualization have been studied by comparing 3D simulation data with velocities from 2D projections of the simulated jet. The satisfactory agreement between the two procedures has allowed to valid our 2D analysis method.

Similarly, the DNS results of the probability of presence of dispersed liquid elements have the same decreasing behaviour as observed in the experimental jet. Nevertheless, the amplitudes are different.

The lack of statistic and the very low speed of the dispersed elements, from the simulation point of view, are related to these deviations.
The core jets were also compared, in terms of interface complexity. A variable based on the average curvature distribution along the spray was defined and showed that the primary atomization is not correctly caught by DNS. Indeed, the complexity increases continuously in the experimental jet, whereas after an abrupt growth, the complexity remains constant in the simulated jet. A study on experimental images by enlarging the field of view is needed to verify if such complexity saturation exists in the experimental spray.

Acknowledgments

This work was supported by the French Agence Nationale de la Recherche (ANR) under reference ANR-13-TDMO-0003. The numerical simulations were carried out at the IDRIS and CRIHAN computational centers.

References

1. Dumouchel C. On the experimental investigation on primary atomization of liquid streams. *Exp Fluids*. 45:371–422, 2008.
2. Sedarsky D, Idlahcen S, Rozé C and Blaisot J. Planar velocity analysis of Diesel spray shadow images. arXiv:1203.5347 [*physics.flu-dyn*], 2012.
3. Sedarsky D, Idlahcen S, Rozé C and Blaisot J. Velocity measurements in the near field of a Diesel fuel injector by ultrafast imagery. *Experiments in Fluids*. Vol. 54:2, 1-12, 2013.
4. Ménard T, Tanguy S. and Berlemont A. Coupling levelset/VOF/ghost fluid methods: Validation and application to 3D simulation of the primary break-up of a liquid jet. *International Journal of Multiphase Flow*. 33(5):510 – 524, 2007.
5. Lebas R, Ménard T, Beau P. A, Berlemont A and Demouli, F. X. Numerical simulation of primary break-up and atomization: DNS and modelling study. *International Journal of Multiphase Flow*, 35(3):247 – 260, 2009.
6. Boudy F and Seers P. Impact of physical properties of biodiesel on the injection process in a common-rail direct injection system. *Energy Conversion and Management*. Vol. 50, Issue 12, Pages 2905-2912, 2009.
7. Yakhot V, Orszag S. A, Thangam S, Gatski, T. B and Speziale C. G. Development of turbulence models for shear flows by a double expansion technique. *Physics of Fluids A*. Vol. 4, No. 7, pp1510-1520, 1992.
8. Ménard T, Tanguy S and Berlemont A. Coupling levelset/VOF/ghost fluid methods: Validation and application to 3D simulation of the primary break-up of a liquid jet. International Journal of Multiphase Flow. 33(5):510 – 524, 2007.
9. Sussman M, Puckett E G. A coupled level set and volume of fluid method for computing 3D and axisymetric incompressible two-phase flows. J Comput Phys 162:301–37, 2000.
10. Klein M, Sadiki A, Janicka J. A digital filter based generation of inflow data for spatially developing direct numerical or large eddy simulations. Journal of Computational Physics, 186(2), 652-665, 2003.
11. Ménard T, Démoulin F. X, Berlemont A. 3D simulation of the primary break-up of a liquid jet by coupling Level Set / VOF / Ghost fluid methods. *6th International Conference on Multiphase Flow ICMF 2007*. Leipzig, Germany, July 9 – 13, 2007.
12. Bradski G and Kaehler A. Learning OpenCV: computer vision with the OpenCV library. *O'Reilly Media*. 1st edition, ISBN 978-0-596-51613-0, 2008.

13. Lounnaci K, Idlahcen S, Sedarsky D, Rozé C and Blaisot J. B. Structure velocity and entropy analysis for characterization of primary breakup in a Diesel spray. *8th International Conference on Multiphase Flow ICMF 2013*. Jeju, Korea, May 26 - 31, 2013.
14. Blaisot J and Yon J. Droplet size and morphology characterization for dense sprays by image processing: application to the Diesel spray. *Experiments in Fluids*. Volume 39, Issue 6, pp.977-994, 2005.
15. Shavit U and Chigier N. Fractal dimensions of liquid jet interface under break-up. *Atom. and Sprays*. 5, 525-543, 1995.
16. Dumouchel C, Cousin J and Grout S. Analysis of two-dimensional liquid spray images: The surface-based scale distribution. *Jr. of Flow Visual. & Image Process*. 15, pp. 59 – 83, 2009.
17. Mokhtarian F, Khim Ung Y and Wang K. Automatic fitting of digitised contours at multiple scales through the curvature scale space technique. *Computers & Graphics.* 29, 961–971, 2005.

Copyright Statement